Modeling of Partial Discharge Processes in Winding Insulation of Low-Voltage Electrical Machines Supplied by High du/dt Inverters

Niklas Driendl
Institute of Electrical Machines (IEM)
RWTH Aachen University
Aachen, Germany
niklas.driendl@iem.rwth-aachen.de

Florian Pauli
Institute of Electrical Machines (IEM)
RWTH Aachen University
Aachen, Germany

Kay Hameyer
Institute of Electrical Machines (IEM)
RWTH Aachen University
Aachen, Germany

***Abstract*—Increasing DC-link voltages and high inverter slew rates in electrical traction drives may be a serious risk for conventionally designed insulation systems. Resulting overvoltages can cause partial discharges (PD) if the critical voltage inside the insulation system is exceeded. This applies in particular to the winding insulation, which is predicted to be the weakest point. The critical voltage can be determined using the *Paschen* curve. The partial discharge inception voltage (PDIV) is not only depending on the amplitude of the electric field but also on the timely sequence. Modeling partial discharge processes is an instrument to predict the electrical load on insulation systems and to evaluate possible new design criteria for insulation systems. The presented model uses the volume-time-theory to calculate the PDIV of twisted pairs of enameled wires. The results of the simulation are compared to PDIV measurements for bipolar voltage pulses with short rise times.**

***Index Terms*—electrical machines, insulation system, partial discharge, winding insulation**

I. Introduction

In low-voltage traction drives, the DC-link voltages are increasing to achieve a faster battery charging process keeping the current level constant. Additionally, SiC-MOSFETs are used to increase the switching frequency and reduce power electronic switching losses [1]. The use of SiC-MOSFETs causes higher inverter slew rates ($^{du}/_{dt}$) compared to conventional Si-IGBTs. The resulting overvoltages lead to higher electric fields inside the machine and thus to higher electrical loads on the insulation system [2]–[4]. If the critical voltage inside the insulation system is exceeded, partial discharges can occur. Low-voltage electrical machines are designed to be PD-free at any operation point by standard [5]. The critical voltage can be increased by applying a thicker insulation which decreases the copper filling factor of the machine. If the insulation is exposed to partial discharge, this leads to electrical aging and erosion. After a certain time, depending on parameters such as switching frequency, voltage and material data, the insulation can not longer withstand the electrical load resulting in the breakdown of the insulation [6]. It is known from literature that the winding insulation is usually the weakest element [2]. The expected lifetime for conventional enameled wires reduces to a few hours or less. Another possibility of facing the higher demand on the insulation is to use corona-resistant insulation materials which can withstand electrical loads significantly longer.

The critical voltage for the winding insulation can be calculated using the *Paschen* curve which indicates the relationship of the breakdown voltage and the product of distance and gas pressure. By using an FE-simulation for a model of two adjacent enameled wires, the electric field distribution can be studied and compared to the *Paschen* curve. To incept a PD a so called starting electron must be available to start an electron avalanche [7]. Exceeding the critical voltage means that electrons have sufficient kinetic energy to ionize molecules. Electrons are accelerated along the electric field lines. If the electrons collide with gas molecules, the molecules can be ionized releasing electrons from their outer shells resulting in an electron avalanche. The electrons collide with the insulation causing damage by breaking up the polymeric bonds.

For a transient voltage, particularly for a switched voltage with a high slew rate, the timely sequence of the applied voltage has to be studied [8]. Therefore, the volume-time-theory is used to estimate the generation of initial electrons to incept a PD. A probability model is used to calculate the risk of PD inception. The electrons can be detached from O_2-molecules or from the insulation surface by field emission.

To validate the simulation model, measurements are performed on twisted pairs of enameled wires representing the winding insulation. The PDIV is measured for different inverter slew rates. In this paper, the test voltage is directly applied to the specimen based on the fact that the first and last turn of a coil can be adjacent to each other constituting the worst-case scenario. To estimate the actual voltage stressing the winding insulation inside the machine, the voltage distribution within the winding has to be calculated based on calculation models as presented in [9]. Additionally, impregnation improving the insulation and increasing the PDIV is not taken into account.

978-1-7281-4878-6/19/$31.00 ©2019 IEEE

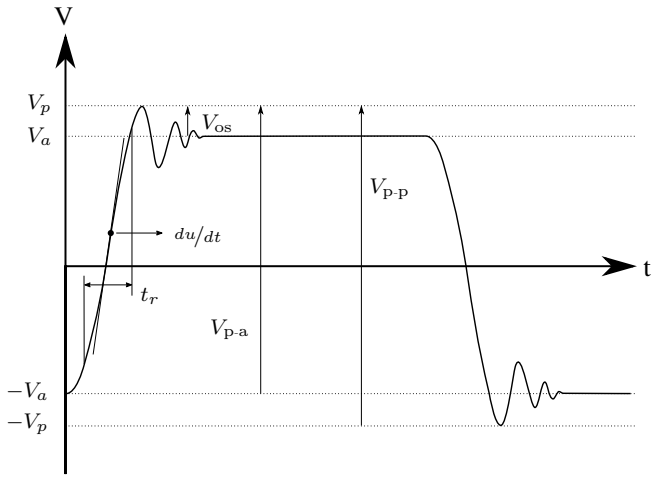

Fig. 1. Bipolar voltage pulse.

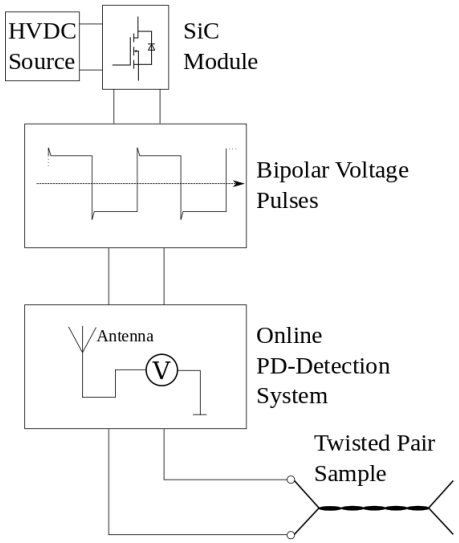

Fig. 2. Measuring setup for partial discharge detection.

II. Measurement of PDIV

In electrical machines used in traction applications, the winding insulation is exposed to bipolar voltages. Overvoltages occur due to the inverter-motor connection and short rise times of the voltage pulses.

A. Definition of Bipolar Voltage Pulse

The quantities of the bipolar voltage pulse are defined in Fig. 1 according to [10]. V_a is defined as the steady-state voltage and corresponds to the DC-link voltage V_{dc}. V_p is the peak voltage including the overshoot voltage V_{os}. The peak-to-peak voltage $V_{\mathrm{p-p}}$ is defined as the difference between the maximum and minimum voltage. The voltage $V_{\mathrm{p-a}}$ is the maximum voltage difference during the switching operation from $-V_a$ to V_a. The rise time t_r is defined as the time for the voltage rise from $0.1 \cdot V_{\mathrm{p-a}}$ to $0.9 \cdot V_{\mathrm{p-a}}$.

B. Test Circuit

In this paper, the winding insulation is analyzed. For this purpose, the PDIV of twisted pair specimens is measured according to [5]. The test setup is depicted in Fig. 2. It consists of an HVDC source and an SiC-switching circuit introduced in [1] to provide bipolar voltage pulses. Three different SiC-modules with voltage rise times of $40\,\mathrm{ns}$, $80\,\mathrm{ns}$ and $120\,\mathrm{ns}$ are applied. Partial discharges are on-line monitored by an HF-antenna. With this test circuit it is possible to separate the signals caused by partial discharges from other signals (e.g. switching frequency of the SiC-modules and rise time of the voltage pulse) in the frequency spectrum even at high inverter slew rates.

The DC-link voltage is increased by $5\,{}^{V}/_{\mathrm{s}}$ starting at $500\,\mathrm{V}$. For each SiC-module, different values of overvoltage are measured. These values depend on the different rise time. In this paper, the peak-to-peak voltage is measured. Therefore, the DC-link voltage is converted to its corresponding peak-to-peak value. The overshoot factor v_{os} is defined in (1) where V_p and V_{dc} are defined according to Fig. 1.

$$v_{\mathrm{os}} = \frac{2 \cdot V_p}{V_{\mathrm{dc}}} \tag{1}$$

C. PDIV Results

To remove statistical uncertainties, 20 specimens are tested for each rise time at a frequency of $20\,\mathrm{kHz}$. The results of the PDIV measurement are depicted in Fig. 3. It is shown that the peak-to-peak value is significantly higher for a lower rise time. For the highest rise time of $120\,\mathrm{ns}$, the PDIV is measured between $1855\,\mathrm{V}$ and $2070\,\mathrm{V}$. The range of PDIV for the shortest rise time of $40\,\mathrm{ns}$ is between $2515\,\mathrm{V}$ and $2778\,\mathrm{V}$. The difference between the maximum and minimum value of the PDIV results for the different rise time is between $144\,\mathrm{V}$ and $302\,\mathrm{V}$. The corresponding slew rate (du/dt) depending on the PDIV and the voltage rise time is determined with regard to the median. For the lowest rise time, the slew rate is $39\,{}^{kV}/_{\mu\mathrm{s}}$. For $80\,\mathrm{ns}$ and $120\,\mathrm{ns}$, the slew rate is $22\,{}^{kV}/_{\mu\mathrm{s}}$ and $15\,{}^{kV}/_{\mu\mathrm{s}}$, respectively.

Assuming that the material properties of all specimens are identical, a possible reason for the spread of the measuring results can be attributed to the manufacturing tolerances of the enameled wires according to [11]. This assumption is discussed later.

D. PD Pattern

It is known from literature [8,12,13] that partial discharge usually occurs at the rising and falling edges of the voltage pulse. Most of the PDs incept close to the first maximum of the overshoot voltage. For comparison the PD pattern of the measurement is analyzed. Therefore, the first PD during the PDIV measurement occurring at rising edge is tracked. The results are depicted in Fig. 4. For the shortest rise time, most of the PDs incept in the first and second maximum of the overshoot voltage as expected. For the other rise times, it can be seen that most of the PDs still occur close the rising

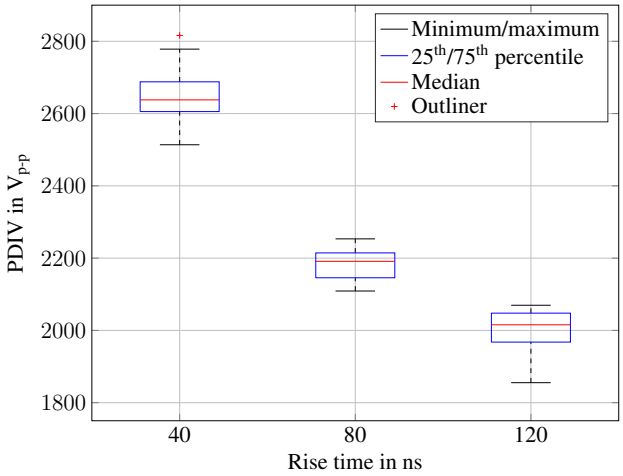

Fig. 3. Results of PDIV measurement.

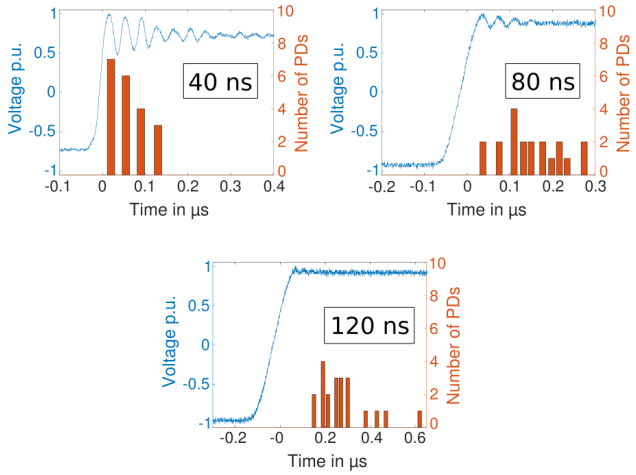

Fig. 4. PD pattern for varying rise time.

edge of the voltage pulse. However, the PDs are more widely distributed, which can be attributed to the smaller overshoot voltage.

From these measurements it can be assumed that the PD pattern is particularly depending on the overshoot characteristic of the voltage pulse which is again depending on the voltage rise time.

III. Modeling of Partial Discharge Processes

Measurements [14] have shown, that the calculation of the PDIV by using the *Paschen* curve corresponds to the measured PDIV under sinusoidal voltage. For a switched voltage, a significantly higher PDIV is measured. The lack of an initial electron is attributed as the cause. Therefore, the transient pattern of the voltage pulse has to be regarded taking into account a fast rise time and overvoltage. In [8] and [15], volume-time theory is used to estimate the generation probability of an initial electron to start an avalanche.

The simulation model consists of two adjacent enameled wires touching each other representing the twisted part of a specimen. The electric field in air is extracted from the FE-simulation and compared to the *Paschen* curve. The relationship between breakdown voltage V_b and gap distance d respectively the gas pressure p is given by (2).

$$V_b = \frac{B \cdot p \cdot d}{\ln\left(A \cdot p \cdot d\right) - \ln\left[\ln\left(1 + \gamma^{-1}\right)\right]} \tag{2}$$

A and B are gas parameters, which are well known for different gases. The parameter γ is known as the second *Townsend* coefficient and describes the feedback effect of the positive ions on the cathode. Effectively, this factor states the number of new starting electrons for subsequent electron avalanches and depends on the combination of gas and cathode material [16].

The first point of intersection between the *Paschen* curve and the extracted solution identifies the critical voltage. In this paper, only normal pressure is regarded. The critical voltage is particularly depending on the insulation thickness, the dielectric constant of the insulation material and the gas pressure. A higher dielectric constant of the insulation material leads to a higher electric field in the air between the conductors and therefore to a lower PDIV as well as a thinner insulation. The distance between the enameled conductors is determined by the length of the electric field lines. As shown in Fig. 5, the points of intersection with the *Paschen* curve indicate, where the critical electric field is locally exceeded. The red-marked critical area can be directly calculated from the dotted field lines. The volume between the critical field lines is evaluated for the case that the local critical electric field is exceeded meaning that a starting electron has sufficient kinetic energy to start an avalanche. Thus, not the whole volume between these field lines is part of the critical volume.

For every voltage, the critical insulation surface and gas volume are calculated, where the critical electric field is exceeded. The electron generation rate is determined by integration across the critical surface S_{cr} and volume V_{cr}, respectively by using (3) and (4).

$$\dot{N}_{\mathrm{e,V}} = \int_{V_{\mathrm{cr}}} \frac{dn_{\mathrm{e,V}}}{dt} \cdot \left(1 - \frac{\eta}{\alpha}\right) dV_{\mathrm{cr}} \tag{3}$$

$$\dot{N}_{\mathrm{e,S}} = \int_{S_{\mathrm{cr}}} \frac{dn_{\mathrm{e,S}}}{dt} \cdot \left(1 - \frac{\eta}{\alpha}\right) dS_{\mathrm{cr}} \tag{4}$$

$dn_{\mathrm{e,V}}/dt$ and $dn_{\mathrm{e,S}}/dt$ are the electron generation rates per volume and surface, respectively. η is the electron attachment coefficient, α is the electron impact coefficient. The term in brackets is known as the *Legler* function. If the local critical voltage is significantly exceeded, the *Legler* function is close to unity due to the fact that $\alpha \gg \eta$ in this case [7]. The surface electron emission rate can be calculated from the *Richardson-Schottky* term stated in (5).

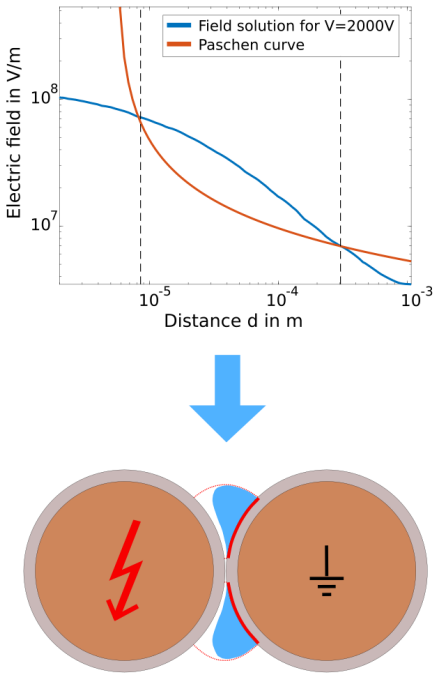

Fig. 5. Comparison of the *Paschen* curve and the extracted solution of the electric field.

$$\frac{dn_{\mathrm{e,S}}}{dt} = \frac{S(T)}{e} \exp\left(-\frac{\phi - \sqrt{\frac{eE}{4\pi\varepsilon_0}}}{kT}\right)\left(1-\frac{\eta}{\alpha}\right) \tag{5}$$

This term consists of the surface area A, the elementary charge e, a temperature dependent function $S(T)$, the effective work function ϕ, the electric field E, the vacuum permittivity ε_0, the Boltzmann constant k, temperature T and the *Legler* function. The electron emission rate is very sensitive to the parameter of the effective work function of the insulation.

The calculation of the volume generation rate is depending on the generation rate of charge carriers and their lifetime [7, 17,18]. The resulting term is a function of the electric field in air.

$$\frac{dn_{\mathrm{e,V}}}{dt} = \frac{n}{1.17\cdot 10^{-4}\mathrm{s}\cdot \exp\left(\frac{2.91\cdot 10^{7} V/\mathrm{m}}{E}\right)} \tag{6}$$

In (6), n is the negative ion density and the denominator is the lifetime of oxygen ions depending on the electric field.

A measured voltage pulse is the simulation input. For every time step, the generation rates are calculated depending on the voltage value and discretely integrated. This is schematically shown in Fig. 6.

A. Probability Model

To evaluate the probability of an initial electron incepting a partial discharge, different models are introduced [8,18].

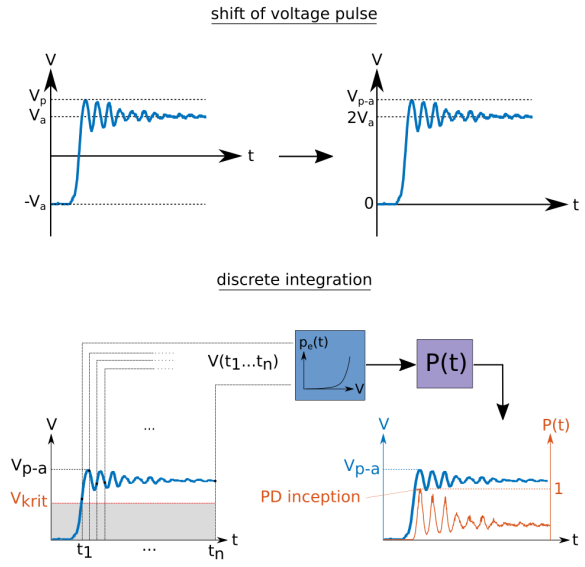

Fig. 6. Schematic discrete integration.

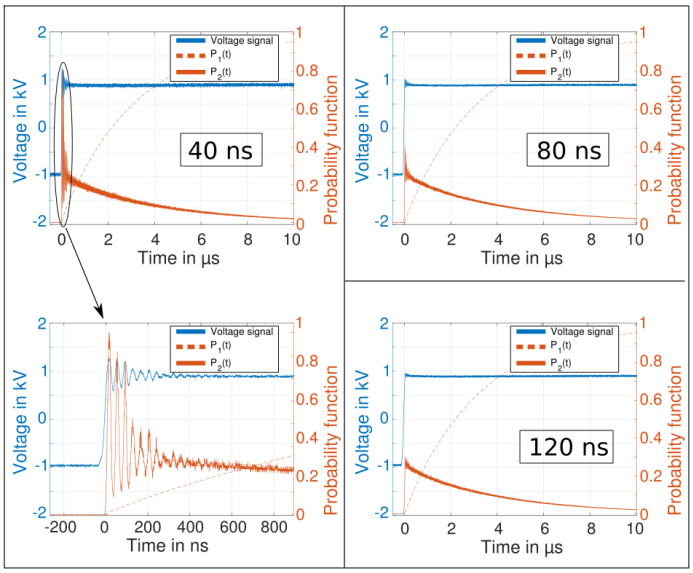

Fig. 7. Transient pattern of the probability functions $P_1(t)$ and $P_2(t)$ for the different rise times.

$$P_1(t) = 1 - \exp\left[\int_0^t p_e(t)\,dt\right] \tag{7}$$

$$P_2(t) = p_e(t)\cdot \exp\left[-\int_0^t p_e(t)\,dt\right] \tag{8}$$

$$\text{with } p_e(t) = \dot{N}_{\mathrm{e,V}} + \dot{N}_{\mathrm{e,S}} \tag{9}$$

The first function stated in (7) develops versus one, if the steady-state voltage V_a is higher than the critical voltage and applied sufficiently long. The threshold value for PD inception is $P_1(t) \geq 0.5$ [8]. Contrary to that, the second function follows a *Poisson* distribution. Inception of PD is regarded for $P_2(t) \geq 1$ [18]. This function converges towards zero

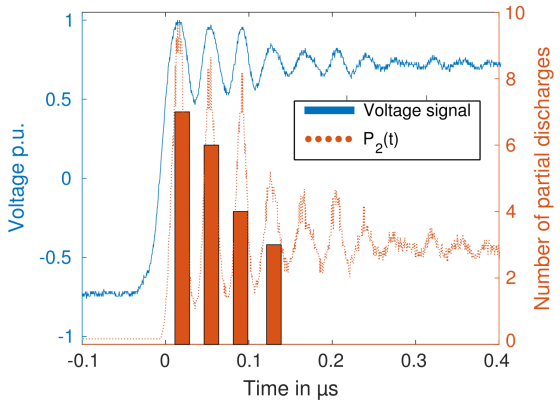

Fig. 8. Comparison of PD pattern and $P_2(t)$ for $t_r = 40\,\mathrm{ns}$.

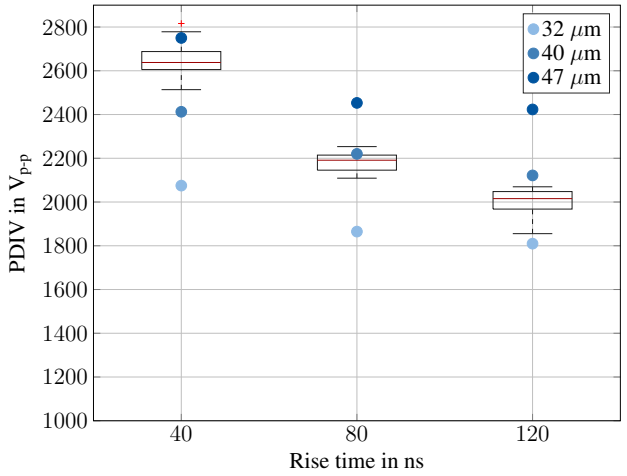

Fig. 9. Results of PDIV simulation compared to measurement results.

due to the exponential term. The transient pattern of the two functions is shown in Fig. 7 for different rise times.

For the first model P_1 the probability of PD inception increases with time. Thus, inception of PD would rather occur at steady state voltage for the regarded voltage amplitude. The probability is mainly depending on the steady-state voltage and pulse width. Function $P_2(t)$ reaches its local maximum values at the peaks of the overshoot voltage. At steady-state voltage the probability of partial discharge inception decreases exponentially with time.

In Fig. 8 the PD pattern (bars) and the probability function $P_2(t)$ (dashed line) are compared for $t_r = 40\,\mathrm{ns}$. This comparison shows a good match of the probability model and the measurement results.

Based on the measurement results and the literature, it can be assumed that partial discharge occurs close to the rising and falling edges of the voltage pulse. Therefore, it can be assumed that the use of function $P_2(t)$ corresponds best to fit the measurement results.

IV. Simulation of PDIV

For the calculation of PDIV, the measured voltage pulses are applied to the simulation model. The PDIV depends on the peak-to-peak value of the applied voltage [19]. In [19] this fact is attributed to space charge accumulation inside the insulation. In this paper, it is assumed that winding insulation is exposed to the full stroke voltage $V_{\mathrm{p-a}}$. Therefore, the bipolar voltage pulse is shifted by V_a for the calculation and regarded as unipolar pulse.

A. Simulation Parameters

The parameters for the *Paschen* curve are listed in Table I.

TABLE I
Parameters of Paschen Curve

Parameter	Unit	Value
A	$(\mathrm{mm}\cdot\mathrm{bar})^{-1}$	1130
B	$\mathrm{kV}\cdot(\mathrm{mm}\cdot\mathrm{bar})^{-1}$	27.4
γ	-	0.0017

The gas parameters A and B for air are well known from literature [20]. Special attention has to be paid on the second electron emission coefficient γ, which depends on the gas-cathode combination. This parameter is experimentally determined in [16] for air and polyamide-imide.

The wire parameters listed in Table II are given by the supplier.

TABLE II
Parameters of Wire

Parameter	Value
Commercial name	Dahrentråht DAMID 200
Conductor diameter	1 mm
Insulation grade[1]	Grade 2
Insulation basecoat	THEIC-modified polyester or polyesterimid (PEI)
Insulation overcoat	Polyamide-imide (PAI)

[1] according to IEC 60317-0-1

The insulation grade and definition refers to the insulation thickness following IEC 60317-0-1 [11]. For wires with a diameter of 1 mm a minimum insulation thickness of 31.5 μm is prescribed. The maximum permitted insulation thickness is 47 μm. Relative permittivities ε_r of 4 (PAI) and 3 (PEI) are estimated as these are typical values for these materials. In [7] the effective work function for weakly conduction material is expected to be in the range of 1.1 eV to 1.3 eV. In [21] the value is determined to 1.28 eV for PEI. This value is used for the simulation.

From test simulations, it could be detected that the influence of volume generation is much lower when compared to surface generation (between 1 % and 5 % depending on the voltage level).

B. Simulation Results

The critical voltage is determined for three different insulation thicknesses resulting in values between 820 V and 990 V. A comparison between measurement and simulation is shown in Fig. 9. For the varying rise time, PDIV is calculated for three

different values of the insulation thickness. The minimum and maximum values refer to the possible manufacturing tolerances following [11]. The simulation results are plotted as the blue points whereas the boxes indicate the measurement results.

It can be seen that the boxes are inside the borders given by simulated PDIV for the lowest and highest value of the insulation thickness. Regarding the average value for the insulation thickness, a good accordance with the measured results for $80\,\mathrm{ns}$ can be observed. For $40\,\mathrm{ns}$ and $120\,\mathrm{ns}$, the simulation results deviate from the measured data. For the largest rise time, a higher PDIV is calculated.

Deviations of the calculated values can be attributed to an inaccurate knowledge of the material data. The simulation model is very sensitive to the effective work constant. The permittivities have a large influence on the electric field in the air between the conductors and thus on the PDIV. Changes in these parameters also affect the sensitivity of the behavior of PDIV and rise time.

V. Conclusions

In this paper, measurements are performed on twisted pairs to find a relationship between the PDIV and the rise time of the inverter voltage. For small rise times, the PDIV is significantly higher when compared to a higher rise time regarding peak-to-peak values. Deviations of measurement results can be attributed to manufacturing tolerances of the wires. Additionally, the PD pattern of the measurement is analyzed for the rising voltage edge showing that PDs incept close to the maximum of the overshoot voltage.

A simulation model based on the volume-time theory is used to calculate the PDIV for fast voltage rise times. Therefore, generation mechanisms due to field emission are regarded. It is found out that the surface generation is the dominant factor. Two different probability models are compared leading to the conclusion that the probability function follows a *Poisson* distribution for switched voltages.

The presented model provides a method to calculate the PDIV of the winding insulation for a bipolar voltage for high values of inverter slew rate. It is shown that a good match of simulation and measurement results is found for a rise time of $80\,\mathrm{ns}$. Further material studies are necessary to increase the accuracy of the simulation model.

References

[1] K. Hameyer, A. Ruf, F. Pauli, “Influence of Fast Switching Semiconductors on the Winding Insulation System of Electrical Machines”, 2018 IEEE International Power Electronics Conference, Niigata 2018.

[2] Fabiani, D.: Accelerated Degradation of AC-Motor Winding Insulation due to Voltage Waveforms Generated by Adjustable Speed Drives, University of Bologna, Diss., 2003.

[3] Florkowska, B. ; Zydron, P. ; Florkowski, M.: Effects of inverter pulses on the electrical insulation system of motors, IEEE, jun 2011. – ISBN 978–1–4244–9310–4, S. 573–578.

[4] A. Ruf, J. Paustenbach, D. Franck and K. Hameyer, A methodology to identify electrical ageing of winding insulation systems, International Electric Machines and Drives Conference, IEMDC 2017, pages CD-ROM, 2017.

[5] IEC 60034-18-41 ed. I, Rotating electrical machines - Part 18-41: Partial discharge free electrical insulation systems (Type I) used in rotating electrical machines fed from voltage converters – Qualification and quality control tests, 2014.

[6] Kaufhold, M.: Failure Mechanism of the Interturn Insulation of Low Voltage Electric Machines Fed by Pulse Controlled Inverters. In: IEEE Electrical Insulation Magazine 12 (1996), September/Oktober, S. 9–16.

[7] Niemeyer, L.: A generalized approach to partial discharge modeling. In: IEEE Transactions on Dielectrics and Electrical Insulation 2 (1995), August, Nr. 4, S. 510–528.

[8] Hayakawa, N. ; Shimizu, F. ; Okubo, H.: Estimation of partial discharge inception voltage of magnet wires under inverter surge voltage by volume-time theory. In: IEEE Transactions on Dielectrics and Electrical Insulation 19 (2012), apr, Nr. 2, S. 550–557.

[9] O. Magdun, S. Blatt, and A. Binder, “Calculation of stator winding parameters to predict the voltage distributions in inverter fed AC machines,” in 9th IEEE International Symposium on Diagnostics for Electric Machines, Power Electronics and Drives (SDEMPED), Aug. 2013, pp. 447–453.

[10] Peng Wang, Hongying Xu, Jian Wang, Wanya Zhou and A. Cavallini, ”The influence of repetitive square wave voltage rise time on partial discharge inception voltage,” 2016 IEEE Conference on Electrical Insulation and Dielectric Phenomena (CEIDP), Toronto, ON, 2016, pp. 759-762.

[11] IEC 60317-0-1, Specifications for particular types of winding wires – Part 0-1: General requirements - Enameled round copper wire, 2013.

[12] Montanari, Gian C. ; Cavallini, Andrea ; Ciani, Fabio ; Contin, Alfredo: Accelerated aging, partial discharges and breakdown of Type II turn-to-turn insulation system of rotating machines. In: 2016 IEEE Electrical Insulation Conference (EIC). Montreal, QC, Canada : IEEE, Juni 2016. – ISBN 978–1–4673–8706–4, S. 190–193.

[13] Wang, Peng ; Xu, Hongying ; Wang, Jian ; Wang, Wei ; Cavallini, Andrea: Effect of repetitive impulsive voltage duty cycle on partial discharge features and insulation endurance of enameled wires for inverter-fed low voltage machines. In: IEEE Transactions on Dielectrics and Electrical Insulation 24 (2017), Nr. 4, S. 2123–2131. – ISSN 1070–9878.

[14] Hayakawa, N. ; Okubo, H.: Partial discharge characteristics of inverter-fed motor coil samples under ac and surge voltage conditions, 2005, S. 5–10.

[15] Norihito Yanagita, Tatsuro Kato, Toshiaki Rokunohe, Takeshi Iwata, Hiroki Kojima, Naoki Hayakawa, Hitoshi Okubo, Development of the Partial Discharge Inception Calculation Model in a Non-uniform Air Gap Considering the Effect of Humidity, IEEJ Transactions on Fundamentals and Materials, 2011, Volume 131, Issue 12, Pages 1017-1023.

[16] Lusuardi, Luca ; Cavallini, Andrea ; Mancinelli, Paolo ; De La Calle Manuel, Gomez ; MartInez-Tarifa, Juan M. ; Robles, Guillermo: Design criteria for inverter-fed Type 1 motors. In: 2016 IEEE International Conference on Dielectrics (ICD). Montpellier, France : IEEE, Juli 2016. – ISBN 978–1–5090–2804–7, S. 605–608.

[17] I. Gallimberti: The mechanism of the long spark formation. Journal de Physique Colloques, 1979, 40 (C7), pp.C7-193-C7-250.

[18] Rokunohe, Toshiaki ; Kato, Tatsuro ; Kojima, Hiroki ; Hayakawa, Naoki ; Okubo, Hitoshi: Calculation model for predicting partial-discharge inception voltage in a non-uniform air gap while considering the effect of humidity. In: IEEE Transactions on Dielectrics and Electrical Insulation 24 (2017), apr, Nr. 2, S. 1123–1130.

[19] Fabiani, D ; Montanari, G C. ; Cavallini, A ; Mazzanti, G: Relation Between Space Charge Accumulation and Partial Discharge Activity in Enameled Wires Under PWM-like Voltage Waveforms. 11 (2004), Nr. 3, S. 13.

[20] Albert II Ernest D. Heylen: Sparking formulae for very high-voltage Paschen characteristics of gases, Electrical Insulation, vol. 22, no. 3, pp. 25–35, May/June 2006.

[21] Hoang, Anh T. ; Serdyuk, Yuriy V. ; Gubanski, Stanislaw M.: Charge transport in a double-layered enamel insulation during surface potential decay. In: IEEE Transactions on Dielectrics and Electrical Insulation 25 (2018), April, Nr. 2, S. 702–712.